# Novel amiloride derivatives that inhibit bacterial motility across multiple strains and stator types

MI Islam[1]*, JH Bae[1]*, T Ishida[2], P Ridone[1], J Lin[1], MJ Kelso[3,4], Y Sowa[2,5], BJ Buckley[3,4], MAB Baker[1,6].

*joint contribution

1. School of Biotechnology and Biomolecular Sciences, University of New South Wales, Sydney, NSW 2052, Australia.
2. Department of Frontier Bioscience, Hosei University, Tokyo, Japan.
3. Molecular Horizons and School of Chemistry and Molecular Bioscience, University of Wollongong, Wollongong, NSW 2522, Australia
4. Illawarra Health and Medical Research Institute, Wollongong, NSW 2522, Australia.
5. Research Center for Micro-Nano Technology, Hosei University, Tokyo, Japan.
6. CSIRO Synthetic Biology Future Science Platform, Brisbane, Australia.

Correspondence: matthew.baker@unsw.edu.au

**Keywords:**

Bacterial motility, bacterial flagellar motor, amiloride, sodium channel blocker, stator.

**Abstract:**

The bacterial flagellar motor (BFM) is a protein complex that confers motility to cells and contributes to survival and virulence. The BFM consists of stators that are ion-selective membrane protein complexes and a rotor that directly connects to a large filament, acting as a propeller. The stator complexes couple ion transit across the membrane to torque that drives rotation of the motor. The most common ion gradients that drive BFM rotation are protons ($H^+$) and sodium ions ($Na^+$). The sodium-powered stators, like those in the PomAPomB stator complex of *Vibrio* spp, can be inhibited by sodium channel inhibitors, in particular, by phenamil, a potent and widely used inhibitor. However, relatively few new sodium-motility inhibitors have been described since the discovery of phenamil. In this study, we discovered two motility inhibitors HM2-16F and BB2-50F from a small library of previously reported amiloride derivatives. Using a tethered cell assay, we showed that both HM2-16F and BB2-50F had inhibition comparable to that of phenamil on Na+ driven motors at matching concentrations, with an additional ability to inhibit rotation in $H^+$ driven motors. The two compounds did not exhibit adverse effects on bacterial growth at the motility-inhibiting concentration of 10 µM, however toxicity was seen for BB2-50F at 100 µM. We performed higher resolution measurements to examine rotation inhibition at moderate (1 µm polystyrene bead) and low loads (60 nm gold bead) and in both the presence and absence of

stators. These measurements suggested that the compounds did not inhibit rotation via direct association with the stator, in contrast to the established mode of action of phenamil. Overall, HM2-16F and BB2-50F showed reversible inhibition of motility across a range of loads, in both $Na^+$ and $H^+$ stator types, and in pathogenic and non-pathogenic strains.

**Importance:**

Here we characterised two novel amiloride derivatives in the search for antimicrobial compounds that target bacterial virulence. Our two compounds were shown to inhibit flagellar motility at 10 μM across multiple strains, from non-pathogenic *E. coli* with flagellar rotation driven by proton or chimeric sodium powered stators, to proton-powered pathogenic *E. coli* (EHEC/UPEC) and lastly in sodium-powered *Vibrio alginolyticus*. Broad anti-motility compounds such as these are important tools in our efforts control virulence of pathogens in health and agricultural settings, as well as providing new compounds to study the inhibited rotation of the flagellar motor.

**Introduction:**

Motility is essential for many bacteria to find nutrients and escape unfavourable conditions (1). Bacterial cells move through liquids or over moist surfaces using rotating flagella, which are driven by the bacterial flagellar motor (BFM) (2). In peritrichous bacteria such as *E. coli*, when the majority of BFMs rotate counter-clockwise, bacteria move linearly (i.e., run) and when one or more BFM rotates clockwise, the helical filament-bundle unravels and bacteria change direction (i.e., tumble) (3). The BFM contains the stator proteins (e.g., MotA and MotB in *E. coli* and PomA and PomB in *Vibrio* spp.), which form an ion transporter on the inner cell membrane, and the rotor proteins (e.g., FliG, FliM, and FliN), that are driven to rotate by torque generation between the stator and rotor (4). Rotation of the BFM is powered by translocation of specific ions (e.g., $H^+$ in *E. coli* and $Na^+$ in *Vibrio* spp.) across the cell membrane through the stator complex (4).

Beside locomotion, motility is crucial during the initial infection and colonisation processes of different pathogenic bacteria (5). Locomotion reduces repulsion between the bacterial cell wall and host tissues, promoting attachment to host cells (6). The importance of motility as a virulence factor was first noted in *Campylobacter jejuni,* when only the motile strain of *C. jejuni* was recovered from an infection site where a mixture of motile and non-motile *C. jejuni* phase variants were used to initiate infection (7). It has since been demonstrated that flagellum-mediated motility promotes the virulence of several gram-negative pathogens, such as for

70 *Bordetella bronchiseptica, B. pertussis* (8)*, Helicobacter sp.* (9)*, Legionella pneumophila* (10),
71 pathogenic *E. coli* strains (11), *Pseudomonas aeruginosa* (12)*, Salmonella typhimurium* (13)*,*
72 and *Vibrio cholerae* (14)*.* Aside from host attachment, flagella also contribute to the formation
73 of biofilms by multiple bacterial pathogens, which promote the development of persistent and
74 chronic infections and antibiotic resistance (1).
75 Amiloride is a diuretic drug and well-characterised inhibitor of the $Na^+$ bacterial flagellar motor
76 (15). Amiloride inhibits rotation of the sodium powered flagellar motor by blocking the
77 translocation of $Na^+$ ions through the channel in a competitive and rapidly reversible manner
78 (16). However, amiloride is of limited utility due to its weak anti-motility activity and adverse
79 effects on other metabolic processes (17). The *N*-phenyl substituted amiloride analogue,
80 phenamil, has been identified as a better inhibitor of sodium powered flagellar motors (17).
81 Phenamil is markedly more potent than amiloride and shows non-competitive inhibition of
82 bacterial motility with slow dissociation (18). Phenamil stops flagellar rotation by binding to a
83 site predicted to lie at the cytoplasmic face of the PomAPomB stator complex (19). Phenamil
84 is a useful tool for flagellar research, but requires high concentrations (>20 μM) and resistant
85 stators can arise from a single point mutation (20, 21). More potent and specific compounds
86 may assist research into stator function and potentially offer leads for new antivirulence drugs.
87 While classical uncouplers can be used to inhibit proton powered motors, they also have
88 adverse effects on cells resulting from collapse of the membrane potential. For example the
89 commonly used uncoupler, carbonyl cyanide *m*-chlorophenyl hydrazone (CCCP), is toxic to
90 both prokaryote and eukaryote cells (22). Here, we report that two recently reported 6-
91 substituted amiloride analogues, BB2-50F and HM2-16F(23, 24) (Fig. 1A), inhibit motility in
92 known phenamil-resistant strains and affect both $Na^+$ and $H^+$ powered flagellar motors.
93
94 **Results:**
95 ***Inhibition of motility***
96 We initially evaluated the anti-motility activity of BB2-50F and HM2-16F along with the
97 control compounds HMA and phenamil using a tethered cell assay (Fig. 1B). We examined the
98 effect of each compound on rotational speed at increasing concentrations (0, 1, 10, and 100
99 μM) against $Na^+$ powered stator, PomAPotB in *E. coli* SYC35 (Δ*motAmotB fliC*$^{sticky}$) strains.
100 Both BB2-50F and HM2-16F inhibited rotation speed in a dose-dependent manner and showed
101 complete inhibition at 10 μM and above (Fig. 1B). The positive control for $Na^+$ -inhibition,
102 phenamil showed similar dose-dependency, with complete inhibition at 10 μM (Fig. 1B). HMA

103 was less potent, with 65% of cells still rotating at 10 μM (Fig. 1B), in agreement with previous
104 findings with other 5-substituted amiloride analogues (16).
105 We further characterised the activity of BB2-50F and HM2-16F alongside phenamil over the
106 concentration range 0−10 μM (Fig. 1C). BB2-50F showed a 2% reduction in the number of
107 rotating cells at 1 μM, 4% at 2.5 μM, 12% at 5 μM, 20% at 7.5 μM and 79% at 10 μM (Fig
108 1C). HM2-16F showed a 6% reduction in the number of rotating cells at 1 μM, 15% at 2.5 μM,
109 28% at 5 μM, 62% at 7.5 μM and 100% at 10 μM (Fig. 1C). In comparison, phenamil produced
110 a 27% reduction in the number of rotating cells at 1 μM, 36% at 2.5 μM, 51% at 5 μM, 58% at
111 7.5 μM and 74% at 10 μM (Fig. 1C). The effect of each compound was reversed following
112 washing with motility buffer.
113 ***Effect on bacterial growth***
114 We measured the growth of *E. coli* SYC35 cells expressing sodium powered stators
115 (PomAPotB) (Supplementary Fig. 1A) and proton powered stators (MotAMotB)
116 (Supplementary Fig. 1B) in the presence of 10 μM and 100 μM BB2-50F and HM2-16F. The
117 rate of growth in both strains was not inhibited relative to vehicle controls for either HM2-16F
118 or BB2-50F at 10 μM (Supplementary Fig. 1). However, at 100 μM the compounds differed in
119 toxicity. HM2-16F reduced the growth rate relative to control over the first five hours in both
120 strains, but did not significantly decrease growth at 15 hr, while BB2-50F completely inhibited
121 growth at 100 μM.
122 ***Effect of $Na^+$ concentration on motility inhibition***
123 We evaluated the inhibition of rotation for BB2-50F, HM2-16F and phenamil while varying
124 the concentration of external sodium to test for $Na^+$ competitive effects (17). Compounds were
125 tested at concentrations of 1−10 μM using motility buffers containing 1, 5, 20, and 85 mM $Na^+$.
126 No significant differences in inhibition were observed for HM2-16F and BB2-50F at the $Na^+$
127 concentrations tested (Fig. 1D). Inhibition was generally flat for BB2-50F between 0-7.5 μM,
128 with a sharp drop seen at 10 μM, whereas HM2-16F inhibition showed a more gradual effect
129 across the range of concentrations tested. In contrast, an exponential decay was seen for
130 phenamil across the concentration range, with the fitted decay constant indistinguishable at all
131 sodium concentrations (Fig 1D, left).
132 ***Activity against phenamil-resistant variants and the proton powered MotA/MotB complex***
133 To assess whether the inhibition of rotation was affected by point mutations known to confer
134 resistance to phenamil, we tested BB2-50F and HM2-16F against known phenamil-resistant
135 mutant constructs at 1, 10 and 100 μM using the tethered cell assay. Four different stator

136 mutants were tested in SYC35: PomA(D148Y) PotB, PomA PotB(P16S), PomA(D148Y)
137 PotB(P16S) and PomA PotB(F22Y/L28Q) (68, 69). Phenamil at 10 μM exhibited no
138 significant effect on the resistant strains (Fig. 2A). In contrast, both compounds showed
139 significant inhibition, completely stopping motility at 10 μM in all phenamil-resistant strains
140 (Fig. 2BC).
141 To further profile the specificity of the inhibitors, we evaluated BB2-50F and HM2-16F against
142 the proton-powered stator complex (MotAMotB) in SYC35. Both HM2-16F and BB2-50F
143 reduced rotation of the proton-powered motor at 10 μM and completely inhibited rotation at
144 100 μM (Fig. 2). In contrast, phenamil did not inhibit MotAMotB stators at concentrations up
145 to 100 μM (Fig. 2).
146 ***Inhibition of motility in other bacterial strains***
147 Inhibition of motility by BB2-50F and HM2-16F was tested in three additional bacterial strains
148 using a free swimming assay that measures the speed of individual cells by videography(25).
149 We first demonstrated inhibition of swimming in MotAMotB and PomAPotB expressing cells
150 (Fig. 3AB), followed by three additional strains: uropathogenic *E. coli* (UPEC)(26) (Fig. 3C),
151 an attenuated enterohemorrhagic *E. coli* (EHEC)(27, 28) (Fig. 3D) and a native sodium
152 swimmer
153 *Vibrio alginolyticus* (29) (Fig. 3E). Both BB2-50F and HM2-16F significantly reduced
154 swimming speed at 10 μM in all strains ($p < 0.05$ in all cases).
155 ***Characterising mechanism of motility inhibition***
156 The activity of BB2-50F and HM2-16F was measured in a bead rotation assay using 1 μm
157 polystyrene bead attached to sticky flagellar filament of JHC36 (Δ*motAmotB* Δ*cheY fliC*$^{sticky}$).
158 This approach reduced the potential for confounding factors that may have affected the tethered
159 cell assay, such as cell-surface adhesion, while also allowing examination of rotation at lower
160 load and at higher speed. Phenamil reduced PomAPotB-driven rotation from 98 ± 7 Hz at 0
161 μM to 7± 3 Hz at 10 μM (Fig. 4A), but had no effect on the proton powered MotAMotB (Fig.
162 4D). In contrast, BB2-50F and HM2-16F reduced the rotation speed of both sodium powered
163 (PomAPotB) and proton powered (MotAMotB) motors to zero at 10 μM (Fig. 4BCF).
164 To assess whether the effects of HM2-16F or BB2-50F were due to direct targeting of the stator
165 complex, we measured rotational diffusion in the presence of drug using the statorless strain.
166 This approach allowed interrogation of whether the compounds were targeting another
167 component of the flagellar motor such as the LP ring or bushing to inhibit rotation. Rotational
168 diffusion for statorless cells remained free in the presence of 10 μM phenamil, indicating no
169 effect on non-stator proteins (Fig. 4G). However, the position of the bead was fixed with

170 minimal rotational or spatial diffusion in the presence of 10 μM BB2-50F (Fig.4H) and HM2-
171 16F (Fig. 4I). This suggested a difference in the mode of action of HM2-16F and BB2-50F
172 compared to phenamil, as these compounds appeared to lock the rotational movement of a 1
173 μm PS bead.
174 To reduce the possibility of measurements being influenced by lingering surface effects from
175 these comparatively large beads, we reduced bead size and composition, and thus mechanical
176 load, by using a 60 nm gold-nanoparticle attached directly to a straightened hook (30). Given
177 the smaller size of the gold bead, and the straightened hook, this system removed possible bead-
178 cell interactions that may have influenced the earlier PS bead assays. Furthermore, the gold
179 nanoparticle assay allows precise measurement of rotation speed at a load close to zero,
180 providing more direct measure of rotor/stator dynamics free from signal damping caused by
181 viscous drag and mechanical loading (31, 32). For this experiment, we used plasmids
182 expressing proton-powered stator MotAMotB (either pSYC28 or pYC409) and the sodium-
183 powered stator PomAPotB (pSHU1234) in SHU174 (Δ*motAmotB* Δ*fliC* Δ*cheY flgE*$_{+GSS+3Cys}$
184 *fliK2798*). The gold nanoparticle measurements indicated that there was no effect of the
185 compounds on motor rotation in either strain at 10 μM (Fig 5D and 5H). However, complete
186 inhibition of rotation was seen for BB2-50F at 100 μM in both systems; the rotation speed was
187 reduced from 770 ±115 Hz to 0 Hz (Fig 5B) and from 270 ± 25 Hz to 0 Hz (Fig. 5D)
188 in PomAPotB and MotAMotB motors respectively. In contrast, HM2-16F did not reduce
189 rotation in either strain up to 100 μM (Fig. 5F and 5H). This result suggests that both BB2-50F
190 and HM2-16F do not directly target the bushing or the rod of the BFM. Upon observing this,
191 tethered cell assays were repeated in the presence of 0.02% w/v Tween-20 to test whether
192 detergent could remove possible hydrophobic interactions between the bead and cell surface
193 that might underlie the broad antimotility effect, but no reduction in inhibition was observed
194 (Supplementary Fig. 2). Overall, this suggests that the effect was not an artefact of
195 non-specific interactions between the bead and cell-surface in the presence of each inhibitor.
196 In contrast, phenamil significantly reduced the rotation speed of PomAPotB containing cells in
197 the gold bead assay at 10 μM (Fig. 5A), in accordance with its direct, non-competitive mode
198 of inhibition described previously.
199 ***Fluorescence of HM2-16F***
200 We expected HM2-16F in particular to have improved fluorescence properties relative to
201 phenamil due to the additional benzofuran group conjugated to the pyrazine. We measured
202 excitation and emission spectra (Supplementary Fig. 4A), and imaged cells in epifluorescence
203 to observe staining with 10 μM HM2-16F (Supplementary Fig. 4B). We further tested HM2-

204 16F using lifetime fluorescence imaging as the quantum yield appeared low (unsuitable for
205 single molecule imaging). We found that the fluorescence lifetime of HM2-16F was 5.4 ± 0.1
206 ns, enabling clear resolution against cellular autofluorescence (1.5 ± 0.1 ns) (Supplementary
207 Fig. 4C).
208
209 **Discussion**
210 Motility is a potential target for new anti-virulence agents (33). Inhibitors are expected to exert
211 less selective pressure than current antibiotics (34), and typically inhibit bacteria at lower
212 concentrations than conventional antibiotics (35). This potentially allows more specific
213 pathogen targeting (e.g. sodium only) as well as lower dosage requirements. Amiloride and its
214 analogues are the best known inhibitors of sodium driven bacterial flagellar motors (16, 17, 36,
215 37). In this study, we evaluated the anti-motility activity of two new amiloride derivatives,
216 BB2-50F and HM2-16F using four methods: 1) tethered cell rotation; 2) free-swimming, 3) 1
217 μm bead rotation, and 4) 60 nm gold bead rotation.
218 Complete inhibition of sodium-driven bacterial rotation was observed at 10 μM for BB2-50F,
219 HM2-16F and phenamil, indicating that these compounds show similar potency. The new
220 compounds showed better anti-motility activity at lower concentrations than other reported
221 motility inhibitors for sodium powered motor system, e.g. amiloride and arginine (16, 38).
222 Furthermore, the inhibitory effect of both BB2-50F and HM2-16F (Fig 1D) appeared to be
223 sodium independent, implying that both compounds worked in a non-competitive manner like
224 phenamil, but unlike the $Na^+$ competitive parent amiloride (17). In addition to its activity at
225 low concentrations, HM2-16F also showed increased green fluorescence properties relative to
226 phenamil, enabling the use of epifluorescence and lifetime imaging to measure uptake and
227 release of HM2-16F in treated cells (Supplementary Fig. 4). This finding bolsters its potential
228 applications in, for example, infection diagnostics (39).
229 BB2-50F and HM2-16F did not affect cellular growth at the motility-blocking concentration
230 of 10 μM (Supplementary Fig. 1). Previously a similar result was reported for the motility
231 inhibitor carvacrol, where even at concentrations up to 200 μM, growth remained uninhibited.
232 (35). Restoration of motility following washing supported their non-lethality and reversible
233 inhibition properties. HM2-16F at 100 μM slowed bacterial growth over the first five hours but
234 was no different from untreated cells after 15 hours (Supplementary Fig. 1). In contrast, BB2-
235 50F was toxic at 100 μM, completely inhibiting growth, and likely explaining its consistent
236 anti-motility effect at these concentrations in multiple strains. However total inhibition of
237 rotation in tethered cell assays was observed at a concentration 10-fold lower than this, where

238 no adverse effects on growth were observed (Supplementary Fig. 1). Additionally, BB2-50F
239 and HM2-16F both inhibited phenamil-resistant stator mutants in *E. coli*, and native stators in
240 other strains, both $Na^+$ and $H^+$ powered. This property represents an improvement over other
241 reported proton-powered motility inhibitors that are effective only in *E. coli* and require high
242 concentrations (up to 600 μM) (40).
243 The mechanism of action of these compounds and the reason(s) for their anti-motility activity
244 across multiple bacterial strains is not clear. The tethered cell assay is an excellent approach
245 for measuring variations in the response of individual cells to treatment and for initial
246 compound screening, however it does not provide positional information for the rotor or assess
247 performance at low load (41). To examine the mechanism of inhibition, and to rule out
248 potentially confounding cell-surface effects that may have influenced earlier experiments using
249 tethered cells, we used a 1 μm polystyrene bead assay (42) to examine the effects of BB2-50F
250 and HM2-16F on rotation. We observed that phenamil in some instances slowed, but did not
251 stop, rotation, whereas BB2-50F and HM2-16F periodically stopped rotation (Fig. 4). We
252 further examined the effect on statorless constructs (Fig. 4GHI) and noted that phenamil had
253 no effect on rotational diffusion in the absence of stators, whereas BB2-50F and
254 HM2-16F locked free rotational diffusion of the bead. The likely explanation is that phenamil
255 directly associates with the stator complex, reducing active torque generation when bound, and
256 thus has no effect in the absence of stators. In contrast, the two compounds appear to jam the
257 motor or adhere the bead to the cellular surface, creating transient pauses, or complete stops at
258 higher concentrations.
259 We used the highest resolution measurement currently available for rotation, a 60-nm gold-
260 nanoparticle affixed directly to a straightened hook (30), to further probe the possible
261 mechanism of action of the compounds. The smaller gold nanoparticle, attached to a
262 straightened hook of ~115 nm length, should not interact with cell surface due to the size of
263 the particle and its distance from the cell exterior. Thus, any observed inhibition would
264 potentially indicate drug binding to the LP ring or bushing of the flagellar motor. However, no
265 inhibition of the rotation speeds of the tested strains were seen in the gold bead assay with
266 BB2-50F or HM2-16F at 10 μM, indicating that the effect of both compounds was likely not
267 due to an on-target interaction with the motor. The interaction is presumably not, however, a
268 simple hydrophobic interaction, as the use of detergent to control for confounding hydrophobic
269 interactions or compound precipitation did not change the potency of BB2-50F and HM2-16F
270 in inhibiting rotation (Supplementary Fig. 2). One potential upside to the proposed surface-
271 based interaction of these compound is that presumably these drugs not incorporated into the

272 cytoplasm. This restricts the possibility that they will be targets for efflux pumps and thus will
273 remain effective as anti-motility comppounds against multi-drug resistant bacteria that rely on
274 such pumps(43). Furthermore, considering these compounds have some known anti-metastatic
275 effects(23, 24), these compounds could potentially show promise not only in the treatment of
276 disease but also simultaneously in reducing the virulence of infections that may arise during
277 treatment.
278
279 **Conclusions**
280 We have identified two new amiloride analogues with anti-motility effects at 10 μM
281 concentration in multiple bacterial strains. Whilst the exact mechanism of action of each proved
282 elusive, both compounds were able to inhibit motility in known phenamil-resistant mutants.
283 We have used a wide range of biophysical techniques to rule out possible mechanisms of
284 action: these compounds do not target the stators, the LP ring, or the bushing. Future work can
285 integrate fluorescence measurements with these compounds, and other new derivatives, for
286 targeted drug discovery that aids flagellar research and the development of novel
287 antimicrobials.
288
289 **Material and Methods:**
290 **Chemical:**
291 5-(*N*,*N*-hexamethylene)amiloride (HMA) (UOW), HM2-16F (UOW) and BB2-50F (UOW)
292 were synthesised as described previously (23, 24). Phenamil methanesulfonate salt (Sigma-
293 Aldrich), Chloramphenicol (Sigma-Aldrich), Dimethyl sulfoxide (DMSO) (Sigma-Aldrich)
294 and D-Arabinose (Sigma-Aldrich).
295 **Bacterial Strains and Plasmids and Growth Conditions**
296 The bacterial strains and plasmids used in this study are shown in full in Supplementary Table
297 1. The primary *E. coli* strains used in this work are SYC35 and RP6894. Pathogenic strains
298 include *Vibrio alginolyticus,* Enterohemorrhagic *Escherichia coli* (EHEC) and Uropathogenic
299 *Escherichia coli* (UPEC). All the strains were cultured in LB broth and LB agar [1% (w/v)
300 Bacto tryptone, 0.5% (w/v) Bacto yeast extract, 0.5% (w/v) NaCl, and 2% (w/v) Bacto agar for
301 solid media] at 37°C. According to the selective antibiotic resistance pattern of the plasmids,
302 chloramphenicol (CAM), ampicillin (AMP) or kanamycin (KAN) were added to a final
303 concentration of 25 μg/mL, 50 μg/mL, and 25 μg/mL, respectively. The *V. alginolyticus* strain,
304 NMB136, was grown in VPG medium (1% (w/v) polypeptone, 0.4% (w/v) $K_2HPO_4$, 3% (w/v)

305 NaCl, 0.5% (w/v) glycerol) and was washed by TMN85 (85 mM NaCl, 215 mM KCl, 50 mM
306 Tris-HCl (pH 7.5), 5 mM $MgCl_2$, 5 mM glucose) with appropriate inhibitors.
307

308 **Tethered cell assay:**

309 We measured the rotation speed of the test strains in the presence of different concentration of
310 test compounds and control drugs using tethered cell assays following a previous protocol with
311 some modifications (44). *E. coli* strain SYC35 (Δ*motAmotB fliC*$^{sticky}$) containing plasmids
312 encoding sodium powered PomAPotB (pSHU1234), proton powered MotAMotB (pDB108)
313 and phenamil resistant PonAPotB (pSHU1235, pSHU1236, pSHU1237, and pSHU1249) were
314 inoculated into TB broth [1% (w/v) Bacto tryptone, 0.5% (w/v) NaCl] containing 0.02% (w/v)
315 arabinose and 25 μg/ml chloramphenicol and were grown overnight (17 h) with 180 rpm at 30
316 °C. The overnight cultures were sub-cultured with a 50-fold dilution into fresh TB broth and
317 incubated for 5 h with 180 rpm at 30°C to get more motile cells. At $OD_{600}$ ~0.80, the flagella
318 of the cells were sheared by passing the culture multiple times (~35) through a 26G needle
319 syringe. After shearing the flagella, the cells were washed three times with motility buffer [10
320 mM potassium-phosphate, 10 mM lactic acid, 100 mM NaCl, and 0.1 mM EDTA, pH 7.0].
321 Cells were then attached on tunnel slides and washed sequentially with motility buffer that
322 contained different concentration test compounds (0, 1, 2.5, 5, 7.5, 10, and 100 μM). According
323 to the experiment purpose we used different concentrations NaCl in the motility buffer. The
324 rotational speed of the cells was observed using phase-contrast microscopy (Nikon) and was
325 recorded at 20 frames per second (FPS) through the 40X objective with a camera (Chameleon3
326 CM3, Point Grey Research). Rotational motion of the cells was analysed using Lab view 2019
327 software (National Instruments).

328 **Growth Curve Assays**

329 Growth assays were performed in the presence of predetermined concentration of test
330 compound to evaluate the effect of the compounds on bacterial growth following the previous
331 protocol (45) with slight modification. *E. coli* strain SYC35 transformed with sodium powered
332 (PomAPotB) and protonpowered (MotAMotB) was used. Briefly, overnight cultures of the test
333 strains with $OD_{600}$ 1.0 were diluted 1:100 in 96-well plates (Corning) with fresh LB broth
334 containing different concentrations of HM2-16F and BB2-50F and incubated at 37°C. Plasmid
335 containing strains (pSHU1234 and pDB-108) were grown in presence of 0.02% (w/v) arabinose
336 and 25 μg/mL chloramphenicol, whereas EHEC and UPEC were grown in LB without
337 arabinose or antibiotic. The $OD_{600}$ were measured in a microplate reader (FLUOstar OPTIMA,
338 BMG LABTECH) every hour for 15 h with a brief shaking interval before each measurement.
339 Measurements in 10 μM were repeated and averaged over three measurements, measurements
340 for 100 μM were repeated and averaged over six measurements.

341

342 **Polystyrene bead assay:**

343 Briefly, *E. coli* strain JHC36 (Δ*motAmotB* Δ*cheY fliC*$^{sticky}$) transformed with plasmids encoding
344 sodium powered (PomAPotB) and proton powered (MotAMotB) was grown overnight in TB
345 broth and then sub-cultured with a 50-fold dilution into fresh TB broth and incubated for 5 h
346 with 180 rpm at 30°C to get more motile cells. At $OD_{600}$ ~0.80, the flagella of the cells were
347 sheared by passing the culture multiple times (~35) through a 26G needle syringe. After
348 shearing the flagella, the cells were washed three times with motility buffer [10 mM potassium-
349 phosphate, 85 mM NaCl, and 0.1 mM EDTA, 1% DMSO, pH 7.0]. Then, the glass slide was
350 coated with poly-L-lysine (PLL) (Sigma Aldrich) and incubated for 10 mins and washed with
351 motility buffer and flushed with 1 µm polystyrene bead (Polysciences, Inc) solution. The
352 sample was then washed with motility buffer containing test compound (10 and 100 µM) and
353 the rotational speed was recorded and analyzed using Lab view 2019 software (National
354 Instruments).

355 **Gold-nanoparticle assay:**

356 We used the 60 nm gold-nanoparticle assay to get the more accurate flagellar rotation speed at
357 lowered load using the previous protocol (30) with slight modification. Briefly, the SHU174
358 *E. coli* (Δ*motAmotB* Δ*fliC* Δ*cheY flgE*$_{+GSS+3Cys}$ *fliK2798*) containing plasmids encoding stators
359 was grown and washed with motility buffer [10 mM potassium-phosphate, 10 mM lactate-Na,
360 67 mM NaCl, 0.1 mM EDTA, 1% DMSO, pH 7.0] and prepared as a cell suspension. The cell
361 suspension was later added to the precipitation of gold nano particle (BBI solutions) and
362 incubated for 30 min. After incubation, the cell mixture was washed with motility buffer and
363 put into PLL coated glass chamber. The sample was then washed with motility buffer
364 containing test compound (10 and 100 µM) and the rotational speed was recorded and analyzed
365 using Lab view 2019 software (National Instruments).

366 **Evaluation of fluorescence property of HM2-16F:**

367 The fluorescence of HM2-16F was analysed using fluorescence microscopy. The emission and
368 excitation spectra of the drug was measured using a spectrophotometer (Cary Eclipse). Briefly,
369 the overnight culture of *E. coli* SYC35 strain transformed with pSHU1234 was prepared and
370 washed with motility buffer. Later, the cell suspension was added to PLL-coated glass slide
371 and incubated for 10 mins and again washed with motility buffer. Cells were treated with test
372 compounds by washing with test compound (10 and 100 µM) containing motility buffer.
373 Finally, drug treated cells were imaged in epifluorescence mode using a Elyra Microscope
374 (Zeiss) using a Plan-Apochromat 63x/1.40 Oil DIC M27 objective, 405 nm illumination and
375 BP495-575 + L750 filter sets. Lifetime imaging was executed on Picoquant MicroTime 200

STED equipped with a PMA Hybrid Series Hybrid Photomultiplier Detector. Illumination was provided by 405 nm laser (Diode 450), with a 60x/1.2 UPlanSApo Water Objective.

## AUTHOR CONTRIBUTIONS

MIM, JB, PR, BJB and MABB designed and executed experiments in, medicinal chemistry, microbiology, microscopy, and rotational measurement. JL and MIM, MJK, BJB, MABB executed initial compound screening. TI and YS designed and executed experiments in rotational measurement with polystyrene beads and gold nanoparticles. MABB and BJB supervised the design, execution and writing of the project. All authors contributed to writing and revision of the manuscript.

## ACKNOWLEDGEMENTS

We would like to thank Tohru Minamino, Yong-Suk Che, Myu Yoshida and Rie Ito for helping a construction of strains and plasmids. We would like to thank Jai Tree for providing the EHEC and UPEC strains and thank Seiji Kojima and Michio Homma for providing *V. alginolyticus* strain.

## FUNDING

MJK was supported by Australian National Health and Medical Research Council (NHMRC) Project Grant (APP1100432). YS was supported by JSPS KAKENHI (JP18H02475 and JP20K06564), MEXT KAKENHI (JP19H05404) and Takeda Science Foundation. BJB acknowledges salary support from the Illawarra Cancer Carers. MABB was supported by a UNSW Scientia Research Fellowship, a CSIRO Synthetic Biology Future Science Platform 2018 Project Grant, and ARC Discovery Project DP190100497.

**References:**

1. Duan Q, Zhou M, Zhu L, Zhu G. 2013. Flagella and bacterial pathogenicity. J Basic Microbiol 53:1–8.
2. Armitage JP. 2007. Bacterial TaxisEncyclopedia of Life Sciences.
3. Berg HC. 2008. E. coli in Motion. Springer Science & Business Media.
4. Sowa Y, Berry RM. 2008. Bacterial flagellar motor. Q Rev Biophys 41:103–132.
5. Xiu P, Liu R, Zhang D, Sun C. 2017. Pumilacidin-Like Lipopeptides Derived from Marine Bacterium Bacillus sp. Strain 176 Suppress the Motility of Vibrio alginolyticus. Appl Environ Microbiol 83.

410 6. Yang Q, Defoirdt T. 2015. Quorum sensing positively regulates flagellar motility in
411 pathogenic Vibrio harveyi. Environ Microbiol 17:960–968.

412 7. Black RE, Levine MM, Clements ML, Hughes TP, Blaser MJ. 1988. Experimental
413 Campylobacter jejuni Infection in Humans. J Infect Dis 157:472–479.

414 8. Josenhans C, Suerbaum S. 2002. The role of motility as a virulence factor in bacteria. Int
415 J Med Microbiol 291:605–614.

416 9. Kao C-Y, Sheu B-S, Wu J-J. 2016. Helicobacter pylori infection: An overview of bacterial
417 virulence factors and pathogenesis. Biomed J 39:14–23.

418 10. Arslan-Aydoğdu EÖ, Kimiran A. 2018.
419 http://www.scielo.br/scielo.php?script=sci_abstract&pid=S1517-
420 83822018000100189&lng=en&nrm=iso&tlng=en. Braz J Microbiol 49:189–199.

421 11. Kao CY, Lin WH, Tseng CC, Wu AB, Wang MC, Wu JJ. 2014. The complex interplay
422 among bacterial motility and virulence factors in different Escherichia coli infections. Eur
423 J Clin Microbiol Infect Dis 33:2157–2162.

424 12. DRAKE D, MONTIE TC. 1988. Flagella, Motility and Invasive Virulence of
425 Pseudomonas aeruginosa. Microbiology, 134:43–52.

426 13. Allen-Vercoe E, Sayers AR, Woodward MJ. 1999. Virulence of Salmonella enterica
427 serotype Enteritidis aflagellate and afimbriate mutants in a day-old chick model.
428 Epidemiol Infect 122:395–402.

429 14. McCarter LL. 2001. Polar Flagellar Motility of theVibrionaceae. Microbiol Mol Biol Rev
430 65:445–462.

431 15. Simchowitz L, Cragoe EJ. 1986. Inhibition of chemotactic factor-activated Na+/H+
432 exchange in human neutrophils by analogues of amiloride: structure-activity relationships
433 in the amiloride series. Mol Pharmacol 30:112–120.

434 16. Sugiyama S, Cragoe EJ, Imae Y. 1988. Amiloride, a specific inhibitor for the Na+-driven
435 flagellar motors of alkalophilic Bacillus. J Biol Chem 263:8215–8219.

436 17. Atsumi T, Sugiyama S, Cragoe EJ, Imae Y. 1990. Specific inhibition of the Na(+)-driven
437 flagellar motors of alkalophilic Bacillus strains by the amiloride analog phenamil. J
438 Bacteriol 172:1634–1639.

439 18. Guia A, Leblanc N, Bose R. 1995. Effects of phenamil on potassium and calcium channels
440 of guinea pig ventricular myocytes. J Pharmacol Exp Ther 274:649–656.

441 19. Kojima S, Asai Y, Atsumi T, Kawagishi I, Homma M. 1999. Na+-driven flagellar motor
442 resistant to phenamil, an amiloride analog, caused by mutations in putative channel
443 components. J Mol Biol 285:1537–1547.

444 20. Jaques S, Kim Y-K, McCarter LL. 1999. Mutations conferring resistance to phenamil and
445 amiloride, inhibitors of sodium-driven motility of Vibrio parahaemolyticus. Proc Natl
446 Acad Sci 96:5740–5745.

21. Ishida T, Ito R, Clark J, Matzke NJ, Sowa Y, Baker MAB. 2019. Sodium-powered stators of the bacterial flagellar motor can generate torque in the presence of phenamil with mutations near the peptidoglycan-binding region. Mol Microbiol 111:1689–1699.

22. Terada H. 1990. Uncouplers of oxidative phosphorylation. Environ Health Perspect 87:213–218.

23. Buckley BJ, Aboelela A, Minaei E, Jiang LX, Xu Z, Ali U, Fildes K, Cheung C-Y, Cook SM, Johnson DC, Bachovchin DA, Cook GM, Apte M, Huang M, Ranson M, Kelso MJ. 2018. 6-Substituted Hexamethylene Amiloride (HMA) Derivatives as Potent and Selective Inhibitors of the Human Urokinase Plasminogen Activator for Use in Cancer. J Med Chem 61:8299–8320.

24. Buckley BJ, Majed H, Aboelela A, Minaei E, Jiang L, Fildes K, Cheung C-Y, Johnson D, Bachovchin D, Cook GM, Huang M, Ranson M, Kelso MJ. 2019. 6-Substituted amiloride derivatives as inhibitors of the urokinase-type plasminogen activator for use in metastatic disease. Bioorg Med Chem Lett 29:126753.

25. Nishiyama M, Sowa Y. 2012. Microscopic Analysis of Bacterial Motility at High Pressure. Biophys J 102:1872–1880.

26. Tree JJ, Ulett GC, Ong C-LY, Trott DJ, McEwan AG, Schembri MA. 2008. Trade-off between iron uptake and protection against oxidative stress: deletion of cueO promotes uropathogenic Escherichia coli virulence in a mouse model of urinary tract infection. J Bacteriol 190:6909–6912.

27. Sy BM, Lan R, Tree JJ. 2020. Early termination of the Shiga toxin transcript generates a regulatory small RNA. Proc Natl Acad Sci U S A 117:25055–25065.

28. Dahan S, Knutton S, Shaw RK, Crepin VF, Dougan G, Frankel G. 2004. Transcriptome of enterohemorrhagic Escherichia coli O157 adhering to eukaryotic plasma membranes. Infect Immun 72:5452–5459.

29. Kojima S, Atsumi T, Muramoto K, Kudo S, Kawagishi I, Homma M. 1997. Vibrio alginolyticus mutants resistant to phenamil, a specific inhibitor of the sodium-driven flagellar motor. J Mol Biol 265:310–318.

30. Nakamura S, Hanaizumi Y, Morimoto YV, Inoue Y, Erhardt M, Minamino T, Namba K. 2020. Direct observation of speed fluctuations of flagellar motor rotation at extremely low load close to zero. Mol Microbiol 113:755–765.

31. Nord AL, Sowa Y, Steel BC, Lo C-J, Berry RM. 2017. Speed of the bacterial flagellar motor near zero load depends on the number of stator units. Proc Natl Acad Sci 114:11603–11608.

32. Wang B, Zhang R, Yuan J. 2017. Limiting (zero-load) speed of the rotary motor of Escherichia coli is independent of the number of torque-generating units. Proc Natl Acad Sci 114:12478–12482.

33. Allen RC, Popat R, Diggle SP, Brown SP. 2014. Targeting virulence: can we make evolution-proof drugs? 4. Nat Rev Microbiol 12:300–308.

486 34. Barczak AK, Hung DT. 2009. Productive steps toward an antimicrobial targeting
487 virulence. Curr Opin Microbiol 12:490–496.

488 35. van Alphen LB, Burt SA, Veenendaal AKJ, Bleumink-Pluym NMC, van Putten JPM.
489 2012. The natural antimicrobial carvacrol inhibits Campylobacter jejuni motility and
490 infection of epithelial cells. PloS One 7:e45343.

491 36. Mohr K. 1993. Amiloride and Its Analogs Unique Cation Transport Inhibitors. Edward J.
492 Cragoe jr., Thomas R. Kleyman, Louis Simchowitz. VCH Weinheim — New York —
493 Basel — Cambridge — Tokyo. Date of publication: December 1992. XV, 388 pages. 62
494 figures. 25 tables. DM 189,—, £ 78,—. Pharm Unserer Zeit 22:273–273.

495 37. McCarter LL. 2004. Dual Flagellar Systems Enable Motility under Different
496 Circumstances. Microb Physiol 7:18–29.

497 38. Atsumi T, Yoshimura F, Sugiyama S. 2006. Arginine inhibits Na-driven flagellar motors
498 of alkaliphilic Bacillus. FEMS Microbiol Lett 256:224–228.

499 39. Stone MRL, Butler MS, Phetsang W, Cooper MA, Blaskovich MAT. 2018. Fluorescent
500 Antibiotics: New Research Tools to Fight Antibiotic Resistance. Trends Biotechnol
501 36:523–536.

502 40. Adams LA, Sharma P, Mohanty B, Ilyichova OV, Mulcair MD, Williams ML, Gleeson
503 EC, Totsika M, Doak BC, Caria S, Rimmer K, Horne J, Shouldice SR, Vazirani M,
504 Headey SJ, Plumb BR, Martin JL, Heras B, Simpson JS, Scanlon MJ. 2015. Application
505 of Fragment-Based Screening to the Design of Inhibitors of Escherichia coli DsbA.
506 Angew Chem Int Ed 54:2179–2184.

507 41. Nirody JA, Sun Y-R, Lo C-J. 2017. The biophysicist's guide to the bacterial flagellar
508 motor. Adv Phys X 2:324–343.

509 42. Kasai T, Sowa Y. 2017. Measurements of the Rotation of the Flagellar Motor by Bead
510 Assay. Methods Mol Biol Clifton NJ 1593:185–192.

511 43. Alcalde-Rico M, Hernando-Amado S, Blanco P, Martínez JL. 2016. Multidrug Efflux
512 Pumps at the Crossroad between Antibiotic Resistance and Bacterial Virulence. Front
513 Microbiol 7.

514 44. Sowa Y, Homma M, Ishijima A, Berry RM. 2014. Hybrid-fuel bacterial flagellar motors
515 in Escherichia coli. Proc Natl Acad Sci 111:3436–3441.

516 45. Islam MI, Lin A, Lai Y-W, Matzke NJ, Baker MAB. 2020. Ancestral Sequence
517 Reconstructions of MotB Are Proton-Motile and Require MotA for Motility. Front
518 Microbiol 11.

519

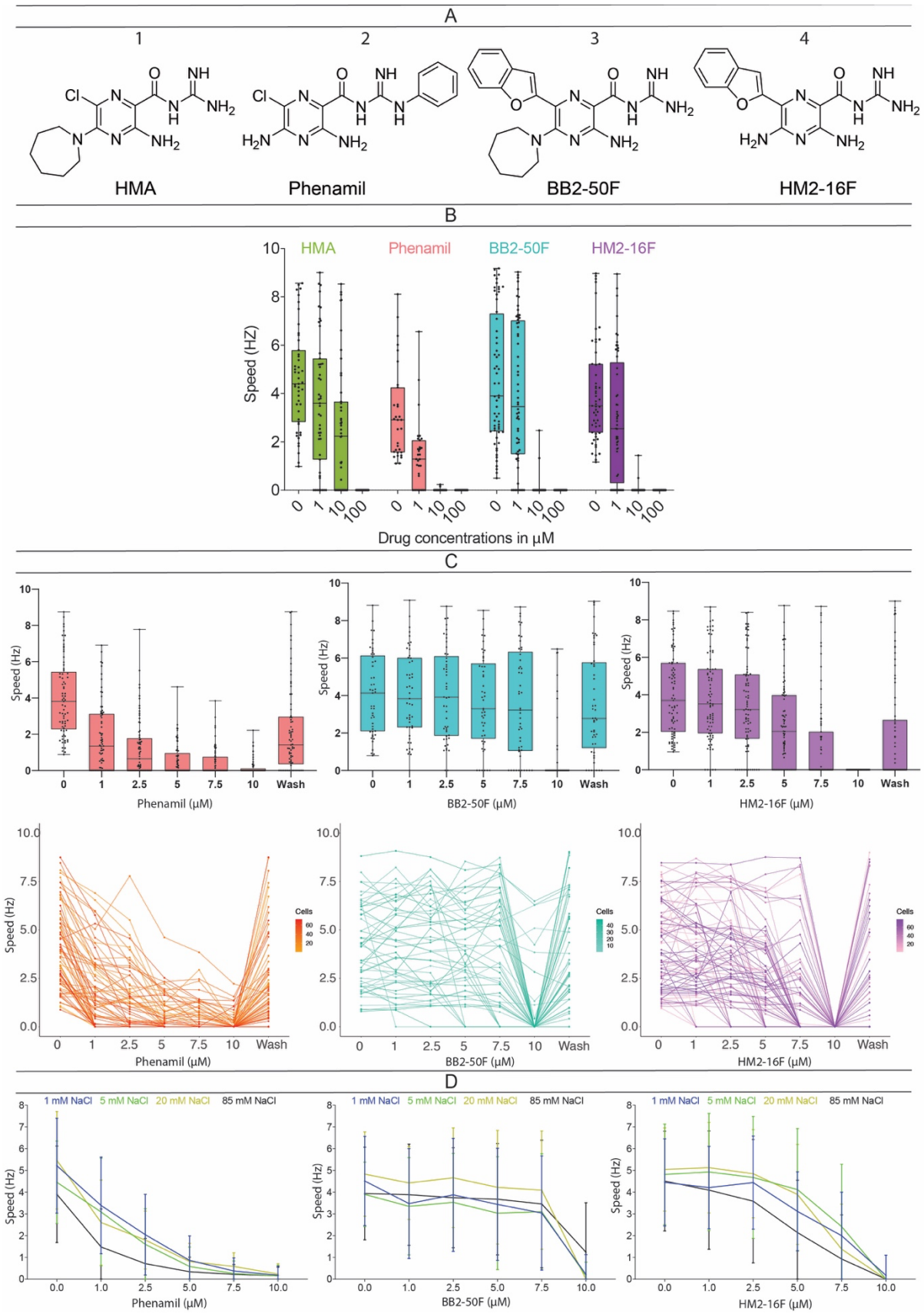


**Fig. 1: Structures and effects of compounds on bacterial rotation in tethered cell assays.** **(A)** Chemical structures of controls 5-*N,N*-(hexamethylene)-amiloride (HMA) and phenamil

523 and test compounds BB2-50F and HM2-16F. **(B)** Tethered cell rotation speed (Hz) after
524 treatment with drugs (μM). Cells were *E. coli* SCY35 strain (ΔMotAB, FliC-sticky) with
525 pSHU1234 (pomApotB). Cells were treated with 0, 1, 10 and 100 μM of each compound.
526 Boxes represent the $25^{th}$ and $75^{th}$ percentile, with median indicated by dividing line. Whiskers
527 cover the full range from minimum to maximum
528 ($n \geq 30$). The lime green bar = HMA, salmon = phenamil, blue = BB2-50F and violet = HM2-
529 16F. **(C)** Dose characterisation of compounds. Cells were treated with 0, 1, 2.5, 5, 7.5 and 10
530 μM of each compound. The line graphs (bottom) indicate the tracking of individual cells'
531 change in rotation speed. **(D)** Effects of sodium concentration ($[Na^+]$) on inhibitory activity.
532 Cells were treated with 0, 1, 2.5, 5, 7.5 and 10 μM drugs diluted in motility buffer containing
533 different $Na^+$ concentrations (1, 5, 20 and 85 mM). Total ionic concentration was held constant
534 and balanced with 84, 80, 65 and 0 mM KCl respectively.
535

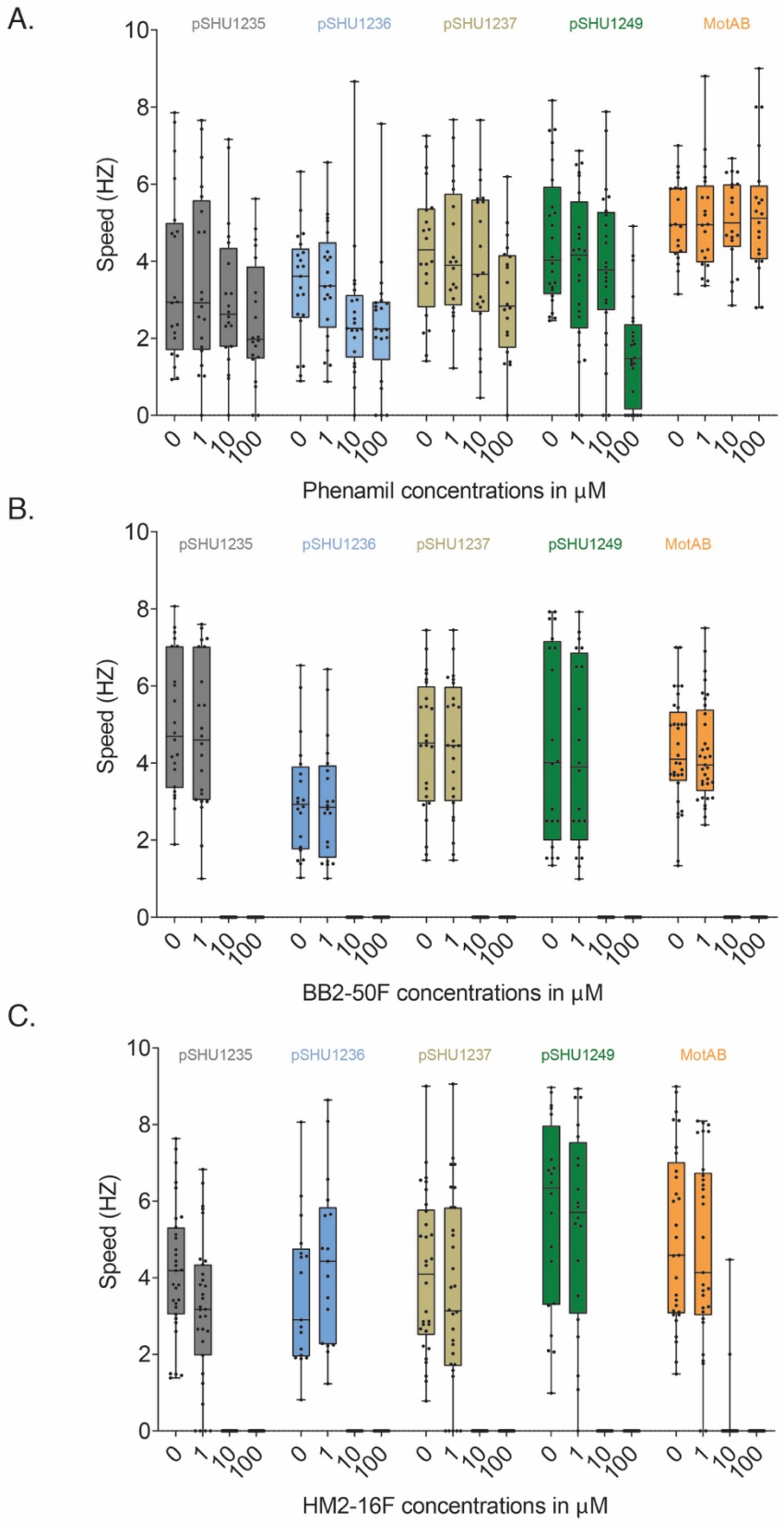


536

537 **Fig. 2:** Activity of compounds against phenamil-resistant stators and proton-powered
538 MotAMotB.

539 Tethered cell speed (Hz) in response to 0, 1, 10, and 100 μM of: **A)** phenamil, **(B)** BB2-50F
540 and
541 (**C**) HM2-16F. Cell used for all assays were *E. coli* SCY35 strain (ΔmotAB, FliC-sticky) with
542 pSHU1235 (PomA (D148Y), PotB), pSHU1236 [PomA, PotB (P16S)], pSHU1237
543 [PomA (D148Y), PotB (P16S)] and pSHU149 [PomA, PotB (F22Y/L28Q)] and pDB-108
544 [MotAMotB] respectively. Boxes represent the 25$^{th}$ and 75$^{th}$ percentile, with median indicated
545 by dividing line. Whiskers depict the full range from minimum to maximum (n≥ 20).

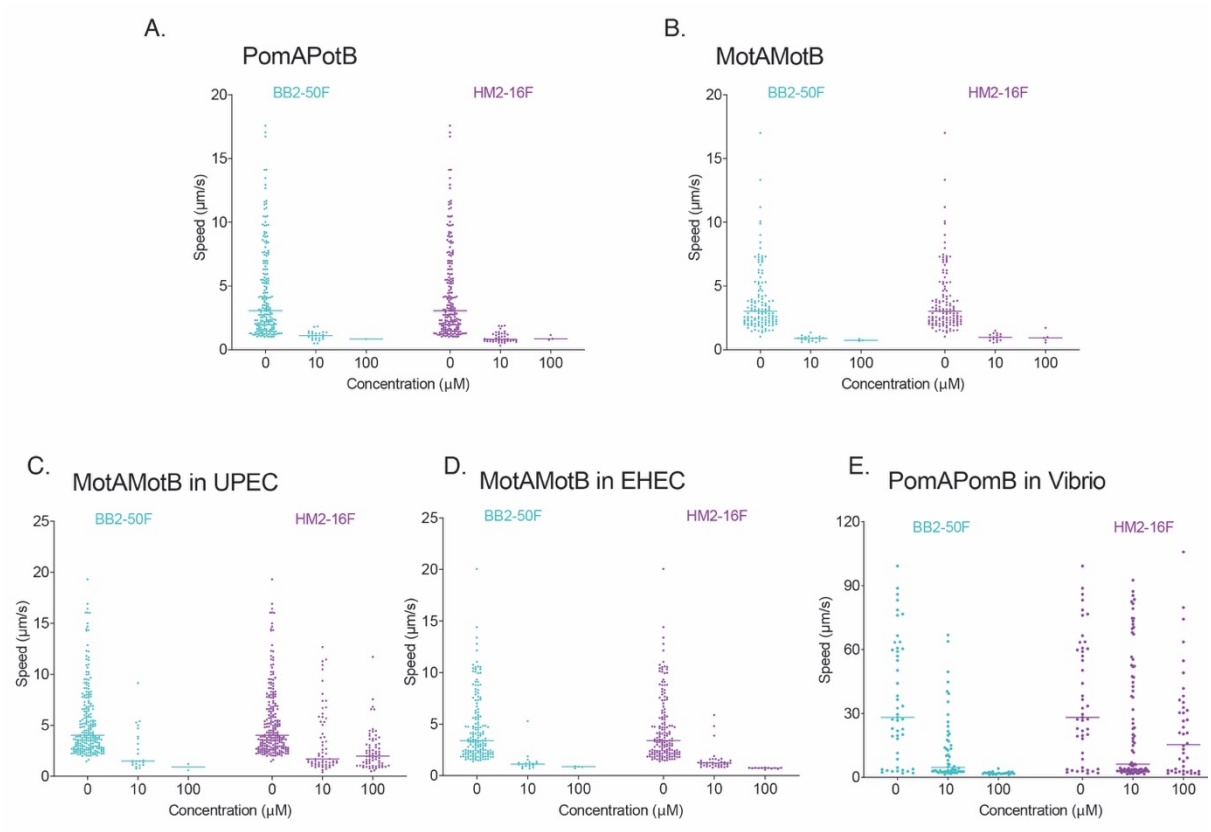


**Fig. 3**: Inhibition of swimming speed by BB2-50F and HM2-16F. Bacterial swimming speed was measured by tracking individual cells using videography in the presence of different concentrations (0, 10, 100 µM) of each compound. Swimming speed of: **(A)** PomAPotB expressed via plasmid in ΔmotAB strain, **(B)** MotAMotB expressed via plasmid in ΔmotAB strain, **(C)** MotAMotB in uropathogenic *Escherichia coli* (UPEC) and **(D)** MotAMotB in enterohemorrhagic *Escherichia coli* (EHEC), and **(E)** PomAPomB in *Vibrio alginolyticus,* all following wash with drug.

Speeds of individual cells shown in µm/s with the scattered plots, median speed indicated by line ($n \geq 30$).

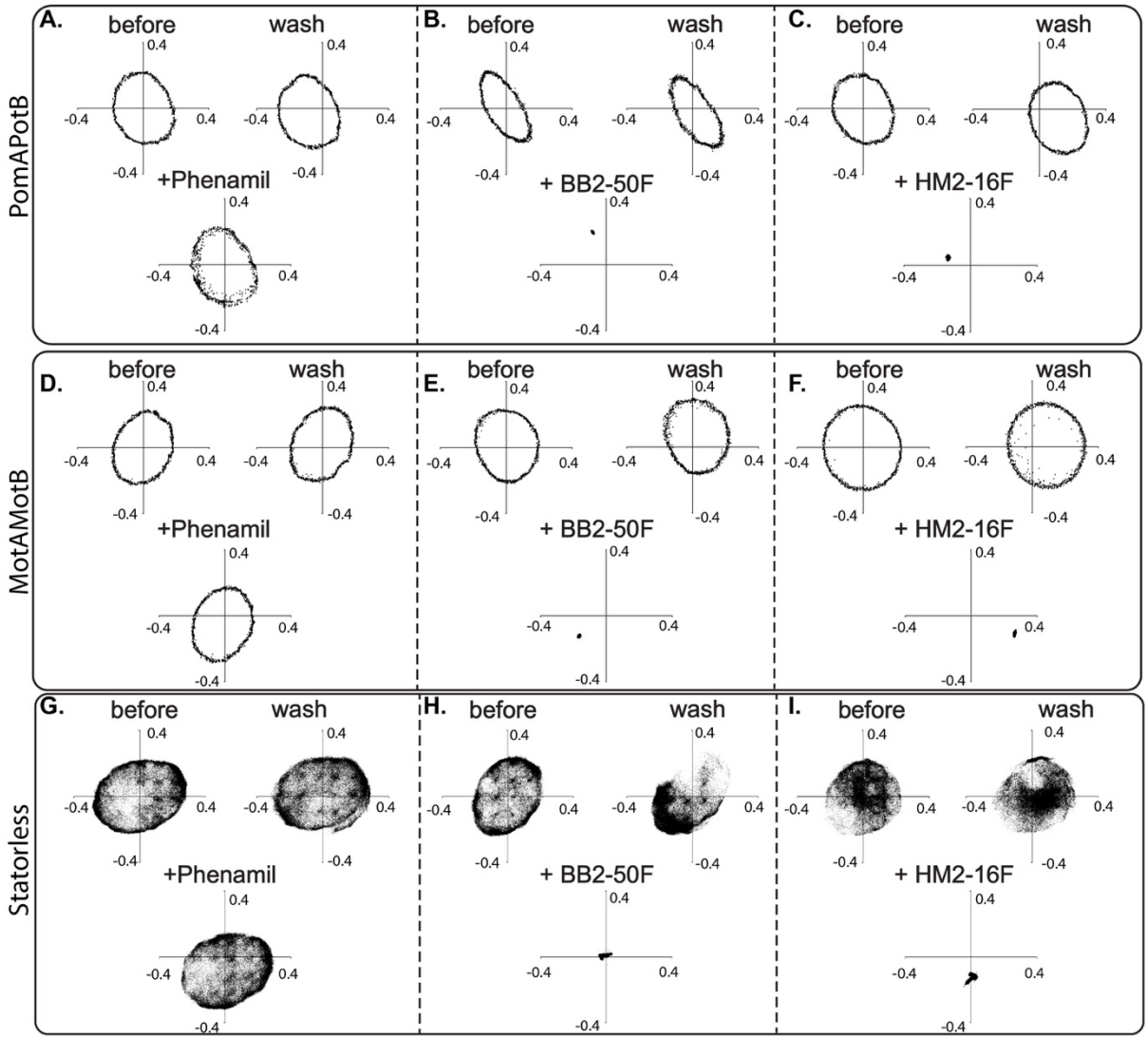


**Fig. 4: Bead assay results for phenamil, BB2-50F and HM2-16F. (top)** 1 µm Polystyrene bead assay in *E. coli* strain JHC36 with plasmid expressed PomAPotB stator (pSHU1234) in presence of (A) phenamil, (B) BB2-50F and (C) HM2-16F. Each panel shows three X-Y scatter plots (over 1 s) of the position a bead attached to the rotating flagellar filament of a single cell before exposure to drug, after exposure to drug, and after wash to remove drug. Raw speed vs time and XY vs time plots shown in Supplementary Fig. 3. **(middle)** Bead assay in *E. coli* strain JHC36 with plasmid expressed MotAMotB stator in presence of (D) phenamil, (E) BB2-50F and (F) HM2-16F. **(Bottom)** X-Y position (over 60 s) for *E. coli* strain JHC36 with no stators expressed. The Brownian diffusion of the bead for 60-120 s is shown before and after treatment with (G) phenamil, (H) BB2-50F and (I) HM2-16F, respectively. All drugs washed in as 50 µL of 10 µM drug, washed out with 200 µL of 85MTB. All lengths in µm.

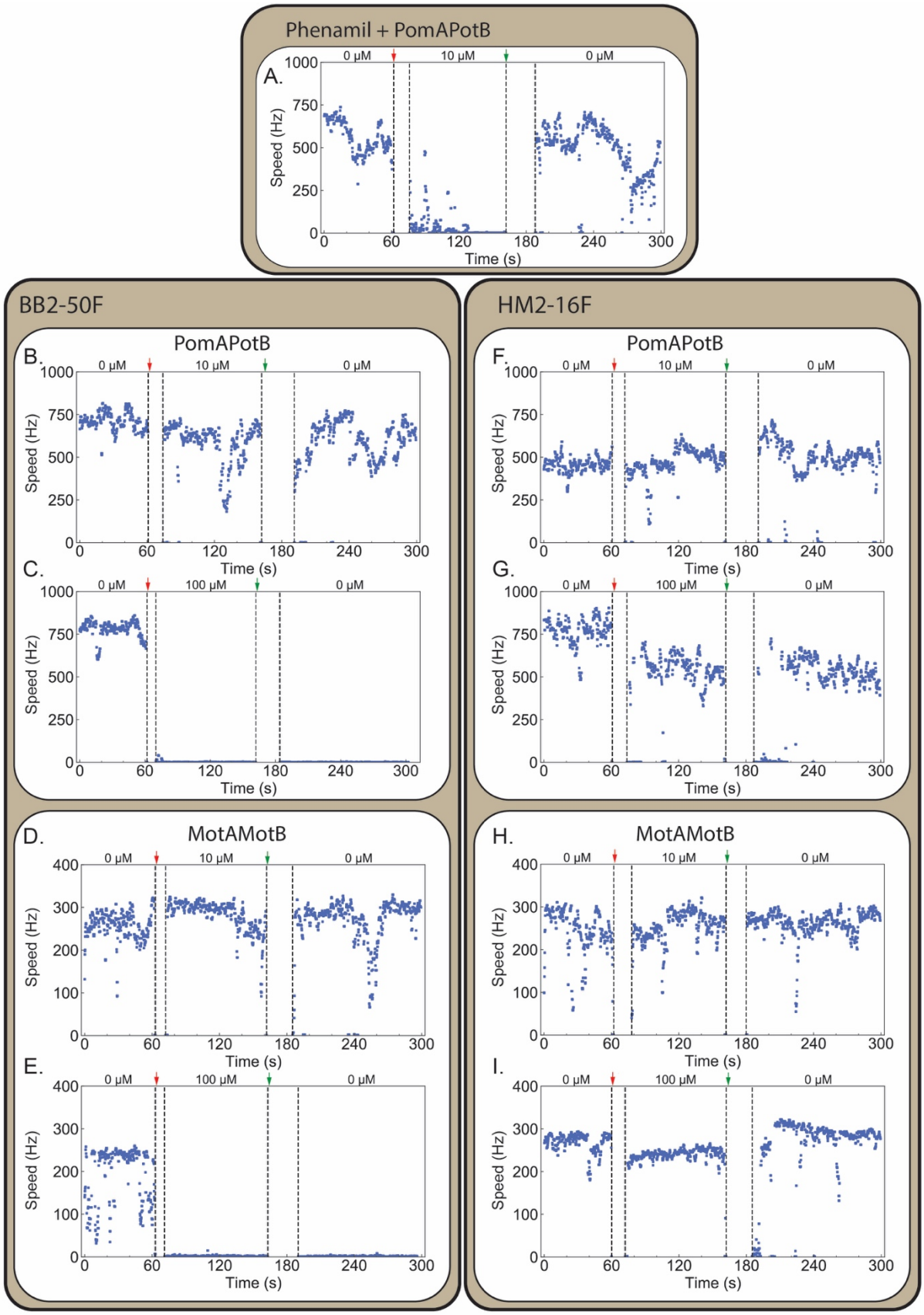


572 **Fig. 5: Gold bead nanoparticle assay results of test compounds.** Speed versus time plots for
573 60 nm gold nanoparticle attached directly to rotating, straightened hook of bacterial flagellar
574 motor before, during and after exposure to drug. Gold nanoparticle assay was performed in

575 SHU174 *E. coli* strain in presence of 10/100 μM BB2-50F (left) and HM2-16F (right) for both
576 PomAPotB and MotAMotB stators, with phenamil action on PomAPotB as a positive control.
577 Red arrow indicates drug flowed in as 50 μL of stated concentration (10 μM or 100 μM), green
578 arrow indicates washout of drug with 200 μL of 67MTB. (A) Positive control for 10 μM
579 phenamil against rotation driven by PomAPotB. Left side: BB2-50F against PomAPotB at (B)
580 10 μM and (C) 100 μM. BB2-50F against MotAMotB at (D) 10 μM and (E) 100 μM. Right
581 side: HM2-16F against PomAPotB at (F) 10 μM and (G) 100 μM**.** HM2-16F against
582 MotAMotB at (H) 10 μM and (I) 100 μM.